



Fabrication of Ag-Ag₂O/reduced TiO₂ nanophotocatalyst and its enhanced visible light driven photocatalytic performance for degradation of diclofenac solution



Yuqi Cui ^{a,1}, Qililing Ma ^{a,1}, Xiaoyong Deng ^a, Qi Meng ^a, Xiuwen Cheng ^{a,c,d,e,*}, Mingzheng Xie ^{a,c}, Xiaoli Li ^a, Qingfeng Cheng ^{b,c,**}, Huiling Liu ^c

^a Key Laboratory of Western China's Environmental Systems (Ministry of Education) and Key Laboratory for Environmental Pollution Prediction and Control, Gansu Province, College of Earth and Environmental Sciences, Lanzhou University, Lanzhou 730000, PR China

^b College of Resources and Environment, Chengdu University of Information Technology, Chengdu 610225, PR China

^c State Key Laboratory of Urban Water Resources and Environment (SKLUWRE), School of Municipal of Environmental Engineering, Harbin Institute of Technology, Huanghe Road 73, Nangang District, Harbin 150090, PR China

^d State Key Laboratory of High Performance Ceramics and Superfine Microstructure, Shanghai Institute of Ceramics, Chinese Academy of Sciences, Dingxi Road, Changning District, Shanghai 2000050, PR China

^e Jiangsu Engineering Technology Research Center of Environmental Cleaning Materials (CEM), Collaborative Innovation Center of Atmospheric Environment and Equipment Technology, School of Environmental Sciences and Engineering, Nanjing University of Information Science and Technology, Nanjing 210044, PR China

ARTICLE INFO

Article history:

Received 11 August 2016

Received in revised form

30 December 2016

Accepted 4 January 2017

Available online 5 January 2017

Keywords:

Ag-Ag₂O/reduced TiO₂

Diclofenac

Visible light

Photocatalysis

Potassium borohydride

ABSTRACT

In this study, Ag-Ag₂O/reduced TiO₂ (denoted as Ag-Ag₂O/r-TiO₂) nano-photocatalyst had been fabricated through one-step solution reduction strategy in the presence of potassium borohydride. Afterwards, physicochemical properties of the resulting samples were investigated by scanning electron microscope (SEM), N₂ adsorption/desorption isotherms, X-ray diffraction (XRD), X-ray photoelectron spectroscopy (XPS), UV-vis diffuse reflectance spectroscopy (UV-vis DRS), electron spin resonance (ESR) and time-resolved surface photovoltage (TR-SPV) techniques. Results indicated that potassium borohydride treatment could simultaneously induce the generation of Ti³⁺ self-doping energy level between the forbidden band of TiO₂ and metallic Ag species existed in the forms of Ag⁰ and Ag₂O nanocrystalline, thereby resulting in the greatly enhanced visible light absorbance and photoinduced charge separation efficiency. In addition, the visible light driven (VLD) photocatalytic (PC) performance was evaluated through the degradation of diclofenac and generation of ·OH radicals. As-expected, Ag-Ag₂O/r-TiO₂ sample exhibited higher VLD PC performance and larger generation amount of ·OH radicals. Furthermore, the enhanced VLD PC mechanism was proposed and confirmed, which was mainly attributed to the synergistic effect originated from the localized SPR of Ag⁰ nanocrystalline and Ti³⁺ self-doping which responsible for the intense visible light absorbance, high photoinduced charge separation efficiency and VLD PC performance.

© 2017 Elsevier B.V. All rights reserved.

1. Introduction

Since the pioneering discovery of water splitting on singlet TiO₂ electrode by Honda in 1972 [1], photocatalytic (PC) oxidation technology has been recognized as one of the most promising

strategies for contaminants elimination, air purification and solar energy conversion [2–4]. Over the past decades, due to the superior PC activity, low-cost and chemical stability, TiO₂ nano-material has been considered as remarkable photocatalyst for waste purification. However, pure TiO₂ nano-catalyst can only be excited by UV light illumination due to its wide band gap energy (for anatase, E_g = 3.2 eV). Nevertheless, in the solar energy spectrum, visible light occupies about 45%, while UV light merely contains 2–4% [5]. Additionally, the high recombination rate of photoinduced electron (e⁻) and hole (h⁺) pairs greatly lowered its PC degradation of contaminants and quantum efficiency of charge carriers [6]. Thus, in order to dissolve the knotty issue of pure TiO₂ nano-material, numerous endeavors on elements doping and coupled other narrow band

* Corresponding authors at: College of Earth and Environmental Sciences, Lanzhou University, Lanzhou 730000, PR China.

** Corresponding author at: College of Resources and Environment, Chengdu University of Information Technology, Chengdu 610225, PR China.

E-mail addresses: chengxw@lzu.edu.cn (X. Cheng), chqf185@163.com (Q. Cheng).

¹ These authors contributed equally to this work.

gap semiconductors have been carried out to effectively utilize the visible light of solar spectrum and enhance its PC performance [7,8].

As demonstrated [9,10], pure TiO₂ nano-material doped with metal ions could induce the band gap narrowing through embedding metal elements into the lattice of TiO₂, resulting in the formation of impurity energy level and remarkable enhanced visible light photoresponse and PC performance. As a model of metal element doping, Ti³⁺ self-doping TiO₂ nano-material has been proven to be a versatile candidate that could significantly improve the light absorbance and PC performance in the visible region [11,12]. However, the reported methods for the generation of oxygen vacancy mainly focused on hydrogen-reduction and high energy particles bombardment [13–15], which often needs harsh fabricating conditions and expensive equipments. Recently, Kang indicated that NaBH₄ treatment could induce the formation of Ti³⁺ species and oxygen vacancy on the surface and interior of TiO₂ nano-material, leading to the greatly improvement of visible light response and H₂ production [16]. Furthermore, our group had fabricated N/Ti³⁺ codoped TiO₂ nano-tubes (TiO₂ NTs) photo-electrode through one-step reduction process in the presence of hydrazine hydrate, which displayed convenient transfer and separation of photoinduced charge carriers [17]. Hence, rational design and facile fabrication of self-doped TiO₂ nano-catalyst through economic strategies have attracted widely attentions.

Recently, some researcher indicted that noble metal nanoparticles, such as Ag, Pt and Au [18–20], could exhibit strong UV-vis absorbance ability due to their surface plasmon resonance (SPR) effect, originating from the collective oscillations of surface electrons. Also, Ag was comparatively cheap and easily synthesized. Therefore, a great deal of efforts has been explored to construct Ag-based plasmonic materials due to the SPR effect of metallic Ag, which can significantly improve the visible light photoresponse and provide new opportunities to develop visible light driven (VLD) photocatalyst [21,22]. At present, Ag/AgX (X = Br, I and Cl) plasmonic nano-catalysts were often designed and synthesized [23,24], while Ag-Ag₂O composite has rarely been reported. Besides these, the current strategies for construction of Ag-Ag₂O composites mainly focused on the template method and deposition process [25,26]. These methods often need harsh conditions and complicated processes, which limited its practical applications.

Very recently, TiO₂ nano-material decorated with multiple metallic elements simultaneously has attracted considerable interest, since it could induce a further enhanced visible light photoresponse and PC performance [27,28]. However, to the best our knowledge, self-doped TiO₂ decorated with Ag-Ag₂O composites has never been reported. Thus, in the present study, Ag-Ag₂O/reduced TiO₂ (denoted as Ag-Ag₂O/r-TiO₂) nano-photocatalyst was fabricated through one-step liquid reduction in the presence of potassium borohydride. Subsequently, microstructure, surface chemical states, optical and photoelectrocatalytic properties of the resulting Ag-Ag₂O/r-TiO₂ nano-photocatalyst were studied systematically. Furthermore, the enhanced VLD PC mechanism for degradation of diclofenac was illustrated and confirmed in detail. As-expected, the as-fabricated Ag-Ag₂O/r-TiO₂ nano-photocatalyst exhibited excellent charge separation efficiency and VLD PC performance.

2. Materials and methods

2.1. Materials

Diclofenac employed as standards and also as pollutants in spiked sample, was purchased from Japan Chemical Co., Ltd. Potassium borohydride (KBH₄), silver nitrate (AgNO₃), terephthalic acid (TA, 99%), *p*-benzoquinone (BQ), ferrous sulfate-ethylene diamine

tetraacetic acid (Fe(II)-EDTA) and *tert*-butyl alcohol (TBA) were analytical grade and kindly purchased from Sinopharm Chemical Reagent Co. LTD. Commercial titanium dioxide (TiO₂) was kindly provided by Degussa Chemical Co., Ltd. Absolute methanol and acetic acid were of HPLC grade. All the chemicals used in this study were analytic grade and were employed without any further purification. Milli Q-water was used throughout during this experiment.

2.2. Fabrication of Ag-Ag₂O/r-TiO₂ nano-photocatalyst

In a typical process, Ag-Ag₂O/r-TiO₂ nano-photocatalyst was constructed through one-step solution reduction process in the presence of potassium borohydride. Firstly, 4.00 g TiO₂ powder was dissolved into 50 mL MQ-water and vigorously stirred for 120 min to get a homogeneous solution. Subsequently, a certain amount of AgNO₃ was added into the above as-formed solution. Then, the resulting TiO₂-Ag⁺ mixture were vigorously shocked for 120 min by sonication treatment when a milk-white solution was formed. Next, to further complete the solution reduction process, 50 mL KBH₄ solution with different concentration ranging from 0.037 to 0.148 mol L⁻¹ was added into the aforementioned TiO₂-Ag⁺ mixture. Afterwards, the tri-component mixture was continuously shocked for 60 min by sonication treatment. Finally, the suspension was washed with MQ-water and then annealed at 873 K for 2 h to obtain the Ag-Ag₂O/r-TiO₂ nano-photocatalyst. For comparison, r-TiO₂ sample was fabricated under the same procedure in the absence of AgNO₃ with the help of 0.130 mol L⁻¹ of KBH₄ solution. It should be noted that Ag/r-TiO₂ sample was also fabricated in the presence of 0.130 mol L⁻¹ of KBH₄ solution without annealing. Besides, Ag₂O/TiO₂ sample was also fabricated from the identical conditions without the addition of KBH₄ solution, and commercial N doped TiO₂ (denoted as N-TiO₂) nano-catalyst was also fabricated for reference according to Asahi's study [29].

Through changing the amount of AgNO₃ and KBH₄ solution, series of Ag-Ag₂O/r-TiO₂ samples were fabricated. They were denoted as X-Ag-Ag₂O/r-TiO₂-Y, where "X" and "Y" represented the amount (g) of AgNO₃ (X = 3.00, 3.50, 4.00, 4.25, 4.50) and concentration (mol L⁻¹) of KBH₄ solution (0.037, 0.063, 0.093, 0.111, 0.130, 0.148), respectively.

2.3. Characterization of Ag-Ag₂O/r-TiO₂ nano-photocatalyst

SEM images of the pure and decorated TiO₂ samples were observed by a Quanta 200F instrument. XRD measurements was recorded on a Rigaku D/MAX III-3B diffractometer with Cu $\text{K}\alpha$ ($\lambda = 0.15406 \text{ nm}$) radiation. The accelerating voltage and applied current were held at 40 kV and 30 mA, respectively. N₂ adsorption-desorption isotherms were conducted on a AUTOSORB-1 (Quantachrome Instruments) at 77 K. It should be noted that the as-fabricated samples had been vacuum-dried at 573 K overnight before measurements. XPS was conducted on a PHI-5700 ESCA instrument with Al $\text{K}\alpha$ X-ray source. All the binding energies (BEs) were calibrated with respect to the C1s peak at 284.6 eV of the surface adventitious carbon. Raman spectra of samples were made operating at 457.9 nm by a HORIBA-Jobin Yvon 800 spectrometer with Ar ion laser beam. UV-vis diffuse reflectance spectra (UV-vis DRS) were measured on a Shimadzu UV-2550 spectrophotometer equipped with an integrating sphere, in which white BaSO₄ was served as the reference. Time-resolved surface photovoltage (TR-SPV) responses of the samples were carried out with a home-built apparatus which had been described in detail elsewhere [30,31]. Fluorescence spectra were recorded by a Hitachi FP-6500 fluorescence spectrophotometer. Electron spin resonance (ESR) was recorded on a BRIAN e-112 instrument.

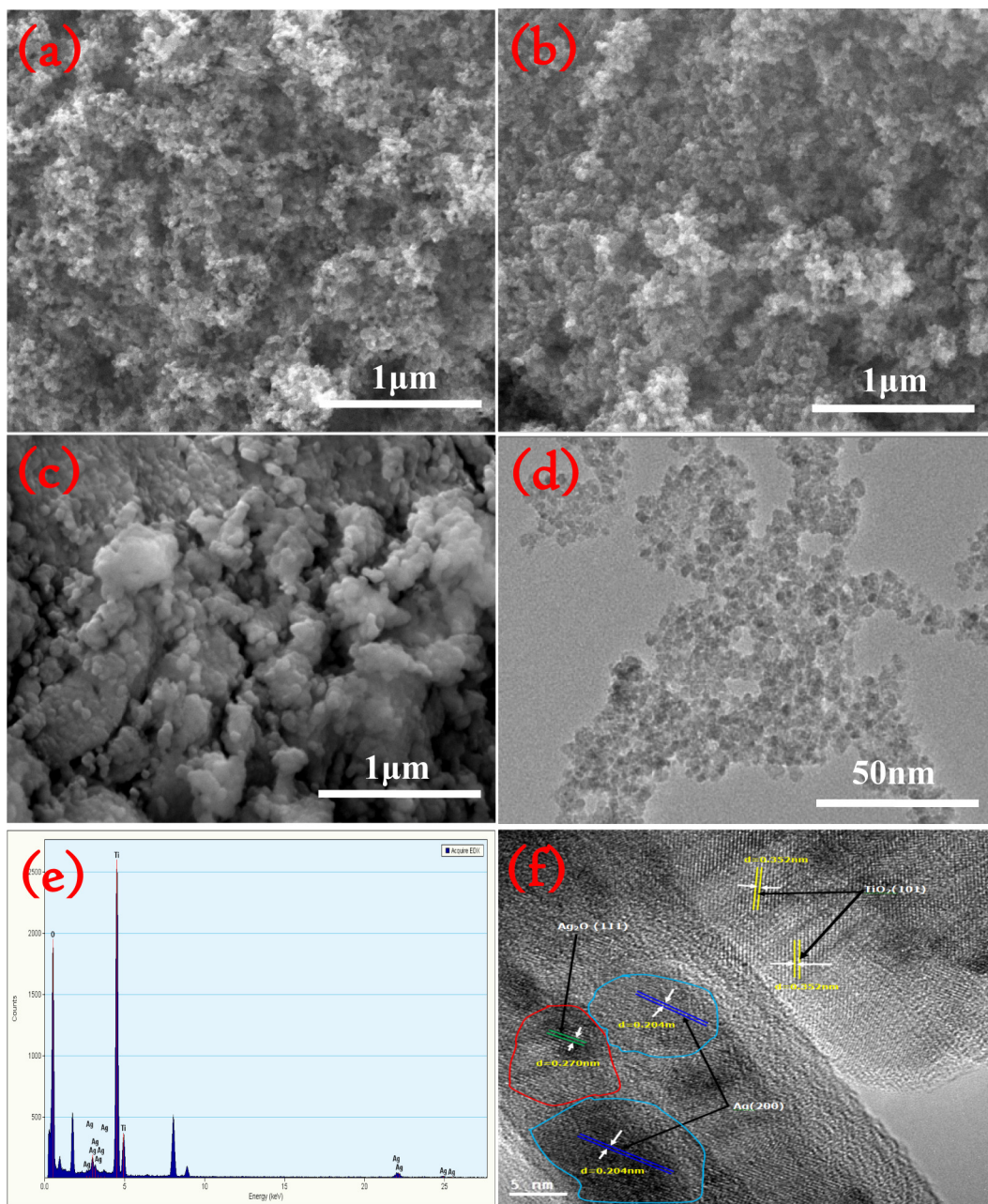


Fig. 1. Top-view SEM images of pure TiO₂ (a), r-TiO₂ (b) and 4.25-Ag-Ag₂O/r-TiO₂-0.130 (c), as well as the TEM image (d), EDX patterns (e) and HRTEM image (f) of 4.25-Ag-Ag₂O/r-TiO₂-0.130 nano-photocatalysts.

2.4. PC performance

Activities of the samples were evaluated by photodegradation of diclofenac under a 350W Xe-arc lamp irradiation. It should be indicated that an UV-cutoff ($\lambda < 400$ nm) and IR-cutoff filter ($\lambda > 800$ nm) was vertically placed aside the photoreactor to ensure the visible light only. Meanwhile, the luminous intensity of Xenon lamp was adjusted to 100 mW cm⁻² by a radiation meter. In each run, 30 mg Ag-Ag₂O/r-TiO₂ sample was added into 100 mL diclofenac solution of 5 mg L⁻¹. Prior to irradiation, the mixed solution was magnetically stirred in dark for 30 min to establish an adsorption-desorption equilibrium. Subsequently, the Xe lamp was switched on. At given time intervals, the collected samples after centrifugation and filtration (0.22 μ m membrane) were measured using a Shimadzu LC 10A high performance liquid chromatography (HPLC) which equipped with a Kromasil KR100-5 C18 column

(150 mm \times 20 mm \times 4.6 mm i.d.). The mobile phase was a mixture of methanol and MilliQ-water (containing 1% acetic acid) with a volume ratio of 75:25. Also, the detection wavelength was 276 nm, and the flow rate was fixed at 1 mL min⁻¹. Besides, in order to determine the degree of mineralization of diclofenac, total organic carbon (TOC) of samples were measured with a Shimadzu TOC-5000 analyzer (catalytic oxidation on Pt at 953 K). Besides, in order to clarify the degradation intermediates of diclofenac, HPLC coupled with a thermo LTQ Orbitrap Discovery mass spectrometer using ESI+/ESI- ionization, operating in full-scan mode, between 50 and 400 umu. Separation was conducted using a Kromasil KR100-5 C18 column (150 mm \times 20 mm \times 4.6 mm i.d.) at a flow rate of 0.3 mL min⁻¹. The other conditions were kept in line with the HPLC measurements. Triplicate analyses were performed for each sample.

3. Results and discussion

3.1. SEM and XRD analysis

In order to observe the morphology transformation of TiO_2 nano-material after reduction treatment and Ag species decoration, top-view SEM images of pure TiO_2 , r- TiO_2 and 4.25-Ag- Ag_2O /r- TiO_2 -0.130 samples were recorded and shown in Fig. 1. As we known [32], P25 TiO_2 had an average diameter of 21 nm and specific surface area of $50 \text{ m}^2 \text{ g}^{-1}$. Also, pure TiO_2 nano-catalyst possessed superior PC activity, which was mainly ascribed to the applicable anatase/rutile proportion (80/20) and high photoinduced charge separation efficiency. Compared with pure TiO_2 (Fig. 1a), r- TiO_2 sample maintained the primitive feature without significant morphological transformation. Furthermore, compared with pure TiO_2 and r- TiO_2 samples, an apparent enlarged diameter for the 4.25-Ag- Ag_2O /r- TiO_2 -0.130 nano-photocatalyst (Fig. 1c) could be obviously observed, which was originated from the decoration of Ag species. Also, it should be noted that the specific surface area of 4.25-Ag- Ag_2O /r- TiO_2 -0.130 and r- TiO_2 was measured to be 49.1 and $49.7 \text{ m}^2 \text{ g}^{-1}$, respectively, demonstrating Ti^{3+} self-doping and surface decoration with Ag species did not remarkably change the adsorption capability of TiO_2 sample. Moreover, TEM image of 4.25-Ag- Ag_2O /r- TiO_2 -0.130 sample was also observed and displayed in Fig. 1d. Clearly, 4.25-Ag- Ag_2O /r- TiO_2 -0.130 had a uniformly sphere-like morphology with an average diameter of 23 nm. Besides, a slight aggregation phenomenon of 4.25-Ag- Ag_2O /r- TiO_2 -0.130 sample could be observed. The EDX patterns (Fig. 1e) confirmed that the as-fabricated sample only contained Ag, Ti and O elements. In order to clarify the relationship of the Ag_2O and Ag particles, high-resolution TEM image of 4.25-Ag- Ag_2O /r- TiO_2 -0.130 was observed, as shown in Fig. 1f. Clearly, the interplanar distance of 0.352, 0.204 and 0.270 nm corresponded to the anatase TiO_2 (101) plane, Ag (200) plane and Ag_2O (111) plane, respectively. Besides, it can also observe that Ag and Ag_2O were in different positions, revealing that they were independent.

Fig. 2 exhibited the typical XRD patterns of 4.25-Ag- Ag_2O /r- TiO_2 -0.130 sample in the range of $15\text{--}65^\circ$ (θ). Meanwhile, pure TiO_2 and r- TiO_2 samples were also conducted as references. Noticeable, all the XRD peaks of TiO_2 -based samples can be well indexed to anatase (JCPDS NO. 21-1272) and rutile (JCPDS NO. 21-1276) [33]. Widely accepted, pure TiO_2 contained both anatase and rutile with anatase phase ($\sim 80\%$) in the majority according to their peak intensities. However, as displayed in Fig. 2, r- TiO_2 sample did not exhibit any additional phase except for anatase and rutile after KBH_4 treatment. Also, the characteristic XRD peak intensity of r- TiO_2 was distinctly increased, demonstrating the improvement of crystallinity. However, for the 4.25-Ag- Ag_2O /r- TiO_2 -0.130 sample, an additional XRD peak at 32.6° was indexed to be (111) crystal facet of Ag_2O phase [34]. Besides, the other two additional peaks at 38.4° and 44.5° were ascribed to (111) and (200) facets of Ag^0 nanocrystallinity [35], respectively. Fig. 2b showed the enlargement of A(101) peaks of pure TiO_2 , r- TiO_2 and 4.25-Ag- Ag_2O /r- TiO_2 -0.130 samples. It can be observed that the diffraction peak position of r- TiO_2 shifted to lower angle (θ) in comparison with the pure TiO_2 , which may be caused by the fact that the ionic radius of the Ti^{3+} (0.67 \AA) was close to that of Ti^{4+} ion (0.61 \AA) in TiO_2 , it is expected that partial Ti^{4+} ion was reduced to form Ti^{3+} , and accordingly, occupied some of the titanium lattice sites, leading to an increment in the lattice parameters and cell volume. However, compared with the XRD patterns of r- TiO_2 , the position of A(101) crystal facet of 4.25-Ag- Ag_2O /r- TiO_2 -0.130 sample did not shift, revealing that Ag species were not weaved into the lattice of TiO_2 but existed in the forms of Ag^0 and Ag_2O nanocrystallines. In order to further confirm the existence and chemical states of the dopants, full profile structure refinement of XRD data

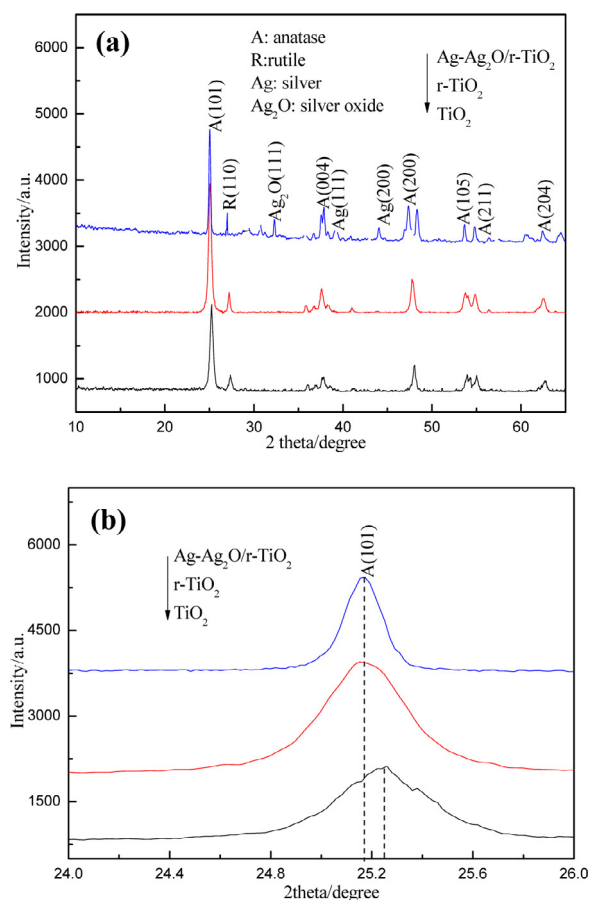


Fig. 2. Full profile XRD patterns (a) and the enlargement of A(101) crystal facet (b) of pure TiO_2 , r- TiO_2 and 4.25-Ag- Ag_2O /r- TiO_2 -0.130 nano-photocatalysts.

using the Rietveld program Muti-Pattern was performed. Results showed that the lattice parameters of pure TiO_2 structure were $a=b=3.7839$ and $c=9.4309$, while the parameters of r- TiO_2 sample were $a=b=3.8053$ and $c=9.4563$, revealing partial Ti^{4+} in the lattice of TiO_2 was reduced by KBH_4 solution. Besides, the cell parameters of 4.25-Ag- Ag_2O /r- TiO_2 -0.130 was calculated to be $a=b=3.8062$ and $c=9.4582$. Thus, we can be concluded that partial lattice Ti^{4+} was reduced to form Ti^{3+} and Ag elements were not weaved into the lattice of TiO_2 but existed as the forms of Ag and Ag_2O nanocrystallines.

3.2. Raman and XPS analysis

Widely accepted, Raman spectroscopy is known as a powerful and effective technique to study the microstructural and surface stoichiometric information of inorganic oxide. Thus, in order to further verify the crystalline structure of 4.25-Ag- Ag_2O /r- TiO_2 -0.130 sample, Raman spectrum was performed and shown in Fig. 3. For comparison, Raman spectra of pure and reduced TiO_2 samples were also measured. As shown in Fig. 3, it can be detected that all the samples displayed five Raman scattering peaks at around 145 , 194 , 394 , 512 and 634 cm^{-1} , corresponding to the Raman active modes of anatase phase with the symmetries of E_g , E_g , B_{1g} , $(A_{1g} + B_{1g})$ and E_g [36], respectively. Surprisingly, from the Raman spectra of three samples, the characteristic Raman peaks of rutile at 235 , 448 and 612 cm^{-1} were not detected [37], revealing that all the samples only contained comparatively slight content of rutile and possessed a main anatase composition. Furthermore, compared with the pure TiO_2 sample, a significant red-shift toward high wavenumber region of E_g (200.5 cm^{-1}), B_{1g} (399 cm^{-1}), $A_{1g} + B_{1g}$

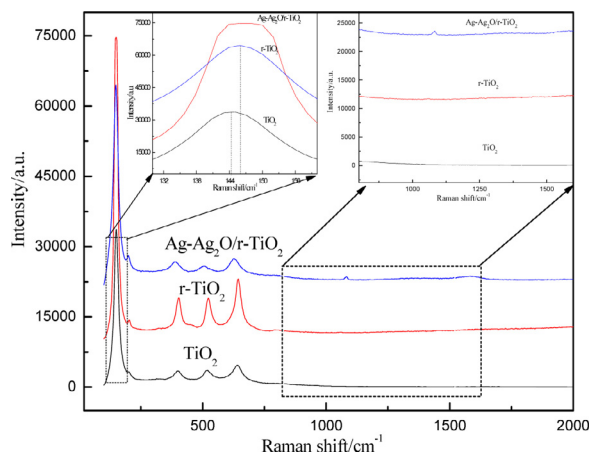


Fig. 3. Raman spectra of pure TiO_2 , r- TiO_2 and 4.25-Ag-Ag₂O/r- TiO_2 -0.130 nano-photocatalysts. Inset showed the enlargement of peaks between 800~1600 cm⁻¹.

(521.2 cm⁻¹) and E_g (640.9 cm⁻¹) bands can be observed for r- TiO_2 and the strongest scattering peak of E_g (146.5 cm⁻¹) became stronger. These results suggested that partial Ti⁴⁺ in the lattice of TiO_2 was substituted by Ti³⁺ species. However, compared with r- TiO_2 , the Raman scattering peaks of 4.25-Ag-Ag₂O/r- TiO_2 -0.130 sample became apparently weaker, which was attributed to the distortion of anatase lattice originated from the Ag metallic SPR effect, which was well agree with the XRD results. In addition, the slight peak located at 1078 cm⁻¹ in the Raman spectra of 4.25-Ag-Ag₂O/r- TiO_2 -0.130 sample was also observed, which was related to the strength of Ag-O model between the Ag and O atoms [38]. Therefore, we can conclude that the triple component 4.25-Ag-Ag₂O/r- TiO_2 -0.130 composite nano-photocatalyst was formed.

The surface chemical states of 4.25-Ag-Ag₂O/r- TiO_2 -0.130 sample were investigated by high-resolution XPS technique and shown in Fig. 4. Seen from the Ag 3d core-level XPS spectrum in Fig. 4a, two major peaks at about 367.2 and 373.2 eV could be clearly observed, which was assigned to Ag3d5/2 and Ag3d3/2 photoelectrons [39], respectively, demonstrating that Ag elements mainly existed as Ag₂O. Besides, two minor peaks at 368 and 374.1 eV could be ascribed to Ag⁰ 3d5/2 and Ag⁰ 3d3/2 [40], respectively, originating from the reduction of Ag⁺ with the help of KBH₄. Hence, the as-constructed Ag-Ag₂O structure could promote the migration of photoinduced electrons and absorbance of visible light photons, consequently improving the separation efficiency of charge carriers and VLD PC performance. Additionally, as exhibited in Fig. 4b, O1s XPS spectra of 4.25-Ag-Ag₂O/r- TiO_2 -0.130 sample were broad and asymmetric, suggesting that there were at least two kinds of chemical states according to the binding energy range from 515 to 545 eV. After fitting, there were three types of oxygen species. The first component with BEs at 528.5 eV was assigned to atomic oxygen with an ionic Ag-O bond [41]. The other two peaks at 530.4 and 532.7 eV were attributed to lattice oxygen and chemisorbed oxygen, respectively. Compared with our previous studies [42], we also observed a red-shift (toward higher binding energy) for O1s XPS peaks, revealing the migration of electrons bound to oxygen and titanium ions towards oxygen vacancies [43]. Thus, it can reasonably be induced that Ag and Ag₂O nanocrystallines were successfully decorated onto the surface of r- TiO_2 , which was in accordance with the XRD and Raman results. Therefore, due to the synergistic effect from SPR of metallic Ag and Ti³⁺ self-doping, we can conclude that 4.25-Ag-Ag₂O/r- TiO_2 -0.130 sample could absorb more visible light photons to participate in the PC reactions, thereby resulting in an enhanced VLD PC efficiency for degradation of refractory organic contaminants. In order to well determine the amount of Ag, Ag₂O and Ti³⁺ in the 4.25-Ag-Ag₂O/r- TiO_2 -

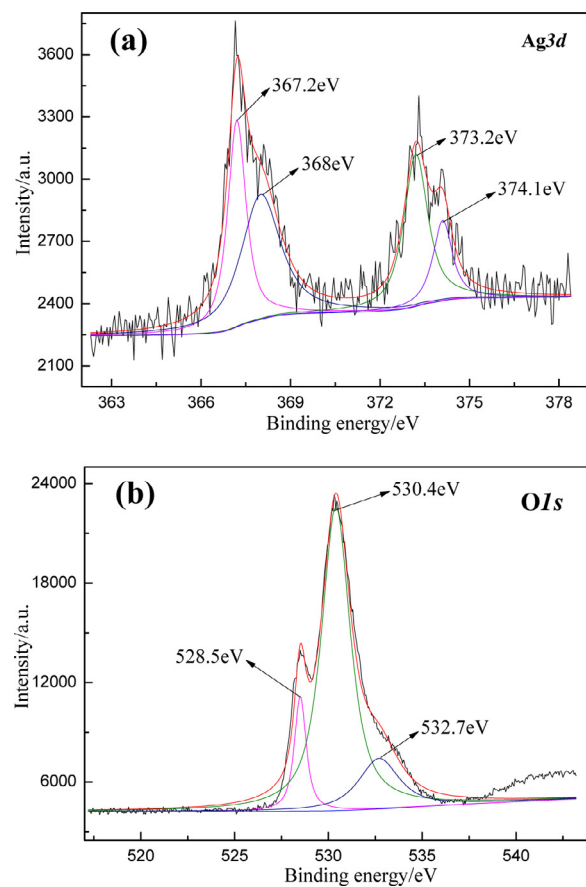


Fig. 4. High-resolution XPS spectra of Ag3d (a) and O1s (b) for 4.25-Ag-Ag₂O/r- TiO_2 -0.130 nano-photocatalyst.

0.130 composite, we used the quantitative formula to calculate the amount of Ag, Ag₂O and Ti³⁺ based on their peak areas and sensitivity factors Ag, O and Ti elements. After calculating, Ag, Ag₂O and Ti³⁺ were found to be 9.1%, 20.9% and 37.8% in the composite, respectively.

3.3. DRS, ESR and TR-SPV analysis

The optical properties of pure TiO_2 , r- TiO_2 and 4.25-Ag-Ag₂O/r- TiO_2 -0.130 samples were all investigated by UV-vis DRS spectra and shown in Fig. 5. Clearly, for both pristine TiO_2 and r- TiO_2

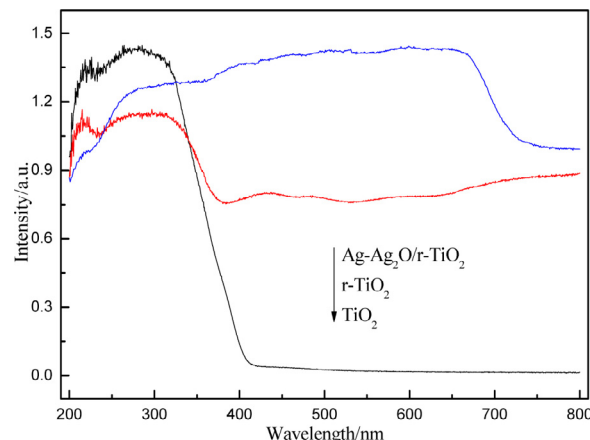


Fig. 5. DRS spectra of pure TiO_2 , r- TiO_2 and 4.25-Ag-Ag₂O/r- TiO_2 -0.130 nano-photocatalysts.

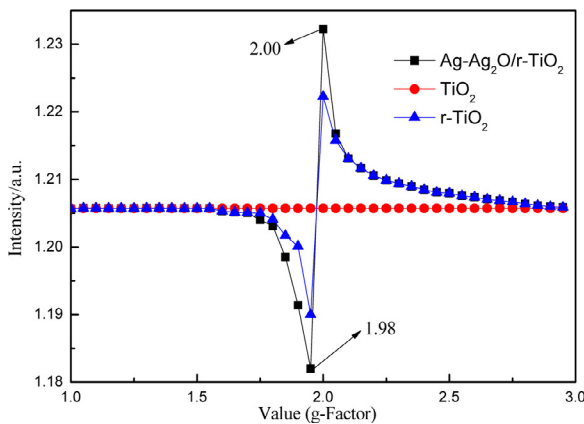


Fig. 6. ESR spectra of pure TiO₂, r-TiO₂ and 4.25-Ag-Ag₂O/r-TiO₂-0.130 nano-photocatalysts.

samples, the onset of absorbance edge was observed at 398 nm, corresponding to the electronic transition from O²⁻ anti-bonding orbital to the lowest empty orbital of Ti⁴⁺ (O2p → Ti3d) [44,45]. However, after reduced by KBH₄ solution, the light absorbance edge of r-TiO₂ was markedly red-shifted to visible region, demonstrating a decrease in band gap energy, which was responsible for the formation of new energy level (Ti³⁺ self-doping energy level) in the forbidden band of TiO₂. Besides these, after decoration with Ag-based plasma species, 4.25-Ag-Ag₂O/r-TiO₂-0.130 sample exhibited intense light absorbance in the whole visible region, which was mainly attributed to the fact that Ti³⁺ self-doping could narrow the band gap energy of TiO₂ for enlarging the photoresponse into visible region and Ag-based plasma could dramatically capture a large number of visible light photons to red-shift the light absorbance, respectively. Therefore, it can be induced that 4.25-Ag-Ag₂O/r-TiO₂-0.130 nano-photocatalyst should possess the highest VLD PC performance.

In order to further confirm the existence of oxygen vacancy and Ti³⁺ species, ESR spectra of r-TiO₂ and 4.25-Ag-Ag₂O/r-TiO₂-0.130 samples were recorded and shown in Fig. 6. Meanwhile, pure TiO₂ was also used as reference. Compared with pure TiO₂ sample, r-TiO₂ and 4.25-Ag-Ag₂O/r-TiO₂-0.130 exhibited two obviously EPR signals at g = 2.00 and 1.98, corresponding to oxygen vacancy and Ti³⁺ [46], respectively. Widely accepted, the surface Ti³⁺ species were unstable in air or water [47], revealing that Ti³⁺ was present in the bulk of TiO₂ rather than on the surface, which was well agreed with the DRS and XPS results.

In order to study the dynamic properties of the photoinduced charge carriers of 4.25-Ag-Ag₂O/r-TiO₂-0.130 sample, time-resolved surface photovoltage (TR-SPV) responses were measured by a laser pulse irradiation with a wavelength of 532 nm. Also, pure and reduced TiO₂ nano-catalysts were measured as references. As demonstrated, photoinduced electron-hole pairs could be immediately separated under a built-in electric field; resulting in a fast SPV component (<10⁻⁵ s) [48]. For n-type TiO₂ nanomaterial, its build-in electric field would contribute to a weak, fast and positive SPV response [49]. Besides, the separation of photoinduced charge carriers is influenced by the carrier diffusion process, which was related to the slow SPV response (<10⁻⁴ s) [50]. Noticeable, as displayed in Fig. 7, all the TiO₂ samples exhibited positive TR-SPV responses, implying that positive holes were generated, separated and then collected on the surface. Seen from Fig. 7, pure TiO₂ sample exhibited a low and short-lifetime TR-SPV response, which was ascribed to the slow charge diffusion process. However, TPV response of TiO₂ sample was obviously increased after surface solution reduction in the presence of KBH₄, revealing the formation of Ti³⁺ self-doping energy level between

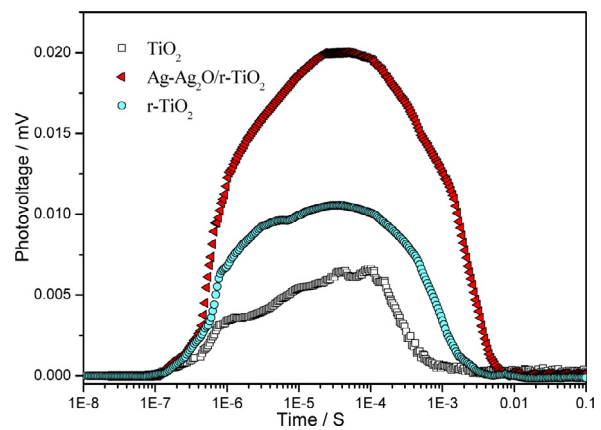


Fig. 7. Time-resolved surface photovoltage responses of pure TiO₂, r-TiO₂ and 4.25-Ag-Ag₂O/r-TiO₂-0.130 nano-photocatalysts.

the forbidden band gap of TiO₂. In particular, the 4.25-Ag-Ag₂O/r-TiO₂-0.130 nano-photocatalyst displayed further improved and lifetime-prolonged TR-SPV response. Accordingly, its charge carrier lifetime was also greatly prolonged by ~ms, corresponding to the synergistic effect of Ti³⁺ self-doping and metallic Ag SPR effect, which favored the visible-excited charge separation and prolonged lifetime. Therefore, it was worthy of noting that 4.25-Ag-Ag₂O/r-TiO₂-0.130 sample should possess longer lifetime and higher separation efficiency of charge carrier, as well as higher VLD PC performance.

3.4. PC performance

As a non-steroidal anti-inflammatory drug (NSAID), diclofenac was commonly used as analgesic, antiarthritic and antirheumatic, and has frequently been detected in municipal wastewater treatment plants (MWTPs) effluents, which was demonstrated to be potentially environmental risk on human beings. Thus, PC performances of Ag-Ag₂O/r-TiO₂ samples were evaluated by degradation of diclofenac solution under visible light irradiation. Meanwhile, the PC performances of r-TiO₂, Ag/r-TiO₂, Ag₂O/TiO₂ and N-TiO₂ samples were also measured as references. Fig. 8a and Fig. 8b showed influence of amount of AgNO₃ and concentration of KBH₄ solution on the PC degradation of diclofenac within 50 min Xenon lamp illumination. Seen from Fig. 8a, we can reasonably conclude that 4.25-Ag-Ag₂O/r-TiO₂-0.130 nano-photocatalyst exhibited the highest PC activity, suggesting that there was an optimum value for Ag-species decoration. The PC activity increased when the amount of AgNO₃ increased, and the PC activity reached the maximum when the amount of AgNO₃ was 4.25 g, which was attributed to the generation of metallic Ag⁰ species. Meanwhile, the as-generated amount of Ag⁰ species was likely suitable for the transfer and separation of photogenerated electron-hole pairs. Furthermore, the PC activity decreased as the further increase of amount of AgNO₃. This phenomenon could be explained by the fact that excessive Ag species would be the recombination center of the photogenerated charge carriers. As displayed in Fig. 8b, the optimum concentration of KBH₄ solution was 0.130 mol L⁻¹. According to the difference of reaction potentials between the equations of Ti⁴⁺ + e → Ti³⁺ and Ag⁺ + e → Ag, Ag⁺ would be more easily reduced. After all the Ag⁺ species were reduced to form Ag, partially lattice Ti⁴⁺ would be reduced to form Ti³⁺ below the conduction band of TiO₂. However, as the further increase of concentration of KBH₄, the PC activity of the obtained sample (4.25-Ag-Ag₂O/r-TiO₂-0.148) decreased inversely. This reason could be explained by the aspect that over-reduction would result in the increase of recombination sites of charge carriers, accordingly leading to a declined

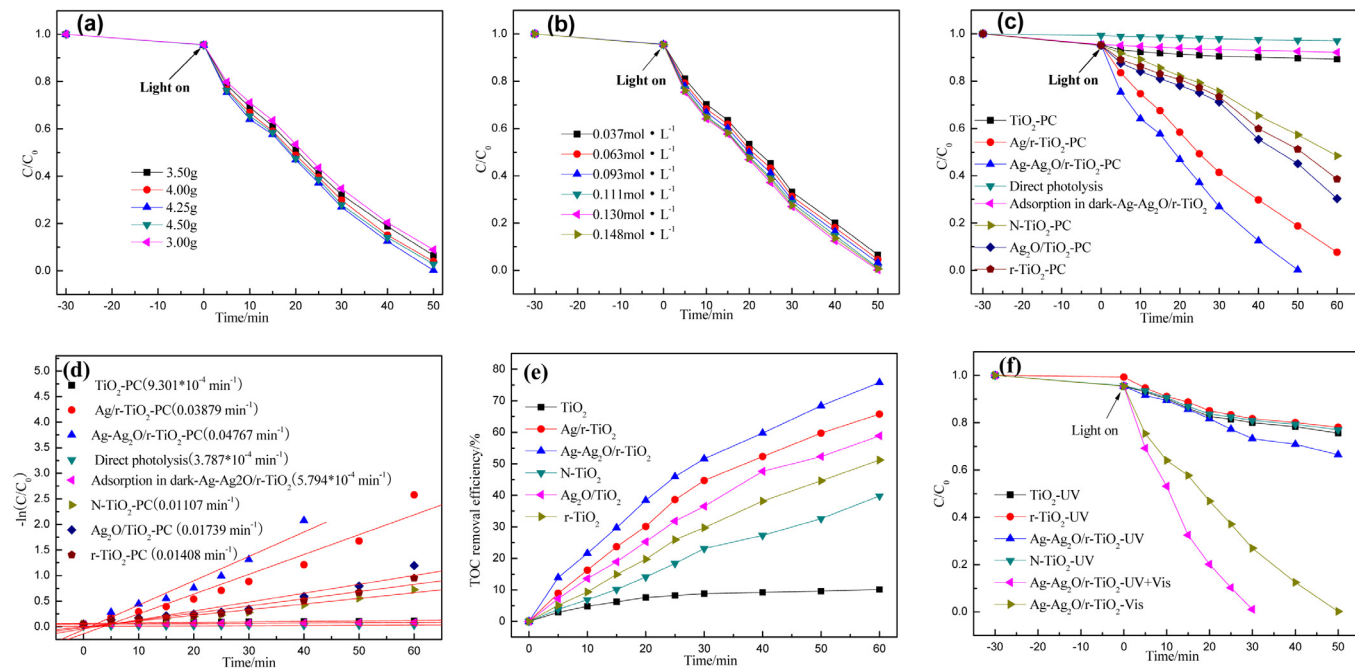


Fig. 8. Influence of amount of AgNO_3 (a) and concentration of KBH_4 (b) on the PC degradation of diclofenac, visible-light-photocatalytic degradation rate (c), the corresponding visible-light-PC evolution curves (d), TOC removal efficiency (e) and UV-excited PC degradation (f) of diclofenac solution on pure TiO_2 , N-TiO_2 , r-TiO_2 , $\text{Ag}_2\text{O}/\text{TiO}_2$, $\text{Ag}/\text{r-TiO}_2$ and 4.25- $\text{Ag}-\text{Ag}_2\text{O}/\text{r-TiO}_2$ -0.130 nano-photocatalysts under simulated sunlight irradiation (the corresponding degradation rate constants are listed in the parentheses in the inset of curve d).

separation efficiency and low visible light PC performance. As exhibited in Fig. 8c, for 4.25- $\text{Ag}-\text{Ag}_2\text{O}/\text{r-TiO}_2$ -0.130 nano-catalyst, only a small amount of diclofenac (<5%) could be degraded through either direct photolysis in the absence of catalyst or adsorption in the dark without any light irradiation. Noticeable, only 10.7% of diclofenac solution could be degraded by pure TiO_2 within 60 min visible irradiation, while 51.6%, 69.7% and 61.4% of diclofenac could be degraded by N-TiO_2 , 4.25- $\text{Ag}-\text{Ag}_2\text{O}/\text{r-TiO}_2$ -0.130 sample, respectively. However, it can be observed that the visible PC efficiency (92.4%) of TiO_2 nano-catalyst was significantly improved by Ag and Ti^{3+} self-doping decoration within 60 min Xe lamp irradiation (for $\text{Ag}/\text{r-TiO}_2$ in our case). Also, 4.25- $\text{Ag}-\text{Ag}_2\text{O}/\text{r-TiO}_2$ -0.130 sample exhibited the highest VLD PC performance, in which 99.8% of diclofenac could be degraded within 50 min visible light irradiation. For the six samples, N-TiO_2 sample exhibited comparative high PC performance due to the improved visible light absorbance originated from the formation of $\text{N}2\text{p}$ localization orbit above the valence band of TiO_2 . Compared with N-TiO_2 [29], r-TiO_2 sample possessed more intense visible light absorbance, corresponding to the higher PC activity. However, $\text{Ag}_2\text{O}/\text{TiO}_2$ displayed higher PC efficiency than that of r-TiO_2 catalyst due to the formation of heterojunctions between the Ag_2O and TiO_2 semiconductors, as well as enhanced visible light absorbance. For $\text{Ag}/\text{r-TiO}_2$, it exhibited high PC activity because of the SPR effect of Ag_0 and Ti^{3+} self-doping energy level. Besides, 4.25- $\text{Ag}-\text{Ag}_2\text{O}/\text{r-TiO}_2$ -0.130 performed the highest PC activity was mainly due to the synergistic effect of intense visible light absorbance and high separation efficiency of photoinduced charge carriers, originating from the synergistic effect of metallic Ag plasma and Ti^{3+} self-doping energy level, which was in accordance with the DRS, ESR and SPS analysis. In addition, kinetics of PC degradation of diclofenac under visible light irradiation over all the TiO_2 catalysts were investigated by applying the Langmuir–Hinshelwood (L–H) model with 60 min [51]. After fitting, the plots $-\ln(C/C_0)$ versus irradiation time t were found to be linear as displayed in Fig. 8d, suggesting that the photodecomposition reactions followed the pseudo-first-order kinetics, in which the apparent reaction rate constants (k)

of pure TiO_2 , N-TiO_2 , r-TiO_2 , $\text{Ag}_2\text{O}/\text{TiO}_2$, $\text{Ag}/\text{r-TiO}_2$ and 4.25- $\text{Ag}-\text{Ag}_2\text{O}/\text{r-TiO}_2$ -0.130 samples were determined to be 9.301×10^{-4} , 0.01107, 0.01408, 0.01739, 0.03879 and 0.04767 min^{-1} , respectively, confirming that 4.25- $\text{Ag}-\text{Ag}_2\text{O}/\text{r-TiO}_2$ -0.130 possessed the highest PC performance for the photodecomposition of diclofenac under visible light irradiation. Furthermore, total organic carbon (TOC) towards to the corresponding diclofenac solution was also measured. Seen from Fig. 8e, it should be clearly noted that 75.8% of diclofenac was mineralized by 4.25- $\text{Ag}-\text{Ag}_2\text{O}/\text{r-TiO}_2$ -0.130 within 60 min visible irradiation, indicating that our catalyst possess high PC performance which can be used as a versatile candidate for wastewater treatment and contaminants purification. In order to further clarify the PC degradation intermediates of diclofenac by 4.25- $\text{Ag}-\text{Ag}_2\text{O}/\text{r-TiO}_2$ -0.130 nano-photocatalyst, HPLC–MS measurements were performed and shown in Fig. S1 and Fig. SII in Supplementary material. It can be concluded that visible-light-PC degradation of diclofenac would undergo three main pathways, including OH-adduct, C–N cleavage of side chain oxidization and firstly decarboxylation of diclofenac, subsequently dechlorination and oxidation. Finally, all the intermediates would be completely mineralized by prolonging reaction time. Generally speaking, Ag plays two roles in enhancing the PC activity including electron acceptor which improved the charge separation efficiency and SPR effect that caused the enhancement of visible light absorbance. Thus, in order to distinguish the contribution of Ag species, an UV-excited experiments were conducted by using a filter ($\lambda > 400 \text{ nm}$). Meanwhile, a full visible–UV light experiment was also carried out for comparison. As shown in Fig. 8f, 21.9% and 24.4% of the PC efficiency for r-TiO_2 and N-TiO_2 samples could be observed, respectively, while 39.7% for 4.25- $\text{Ag}-\text{Ag}_2\text{O}/\text{r-TiO}_2$ -0.130 was obtained within 50 min UV-illumination. However, 99.9% of diclofenac could be degraded by 4.25- $\text{Ag}-\text{Ag}_2\text{O}/\text{r-TiO}_2$ -0.130 within 30 min Xenon lamp (UV and visible light spectrum) illumination. Based on the above analysis, we can concluded that Ag mainly exhibited the SPR effect that caused the enhancement of visible light absorbance, and comparatively lesser to the electron acceptor.

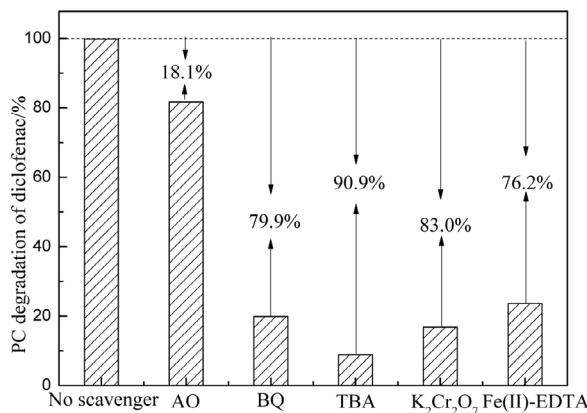


Fig. 9. Effect of each reaction species on PC degradation of diclofenac solution by 4.25-Ag-Ag₂O/r-TiO₂-0.130 nano-photocatalyst.

3.5. Contribution of different reactive species

As demonstrated [17], several reactive species including •OH, $\bullet O_2^-$, H_2O_2 , e^- and h^+ could participate in the PC reactions. Thus, in order to distinguish the contribution of each primary reactive species to the PC efficiency, a series of scavengers were individually added into the reactor during the PC process. Fig. 9 showed the PC efficiency towards the degradation of diclofenac solution within 50 min visible irradiation in the presence of scavengers. Clearly, the PC efficiency was 99.8% after 50 min visible irradiation in the absence of any scavenger. In order to evaluate the role of photoinduced holes (h^+), ammonium oxalate (AO) scavenger was added during the PC process [52]. Obviously, the PC efficiency (81.7%) of diclofenac was moderately decreased, revealing that h^+ could participate in the PC reaction, while exhibited a certain contribution to the PC performance due to the production of •OH radicals originated from the reaction between h^+ and H_2O/OH^- species. Furthermore, when *tert*-butyl alcohol (TBA, •OH scavenger) was added into the PC reaction system [53], the PC efficiency (8.9%) of diclofenac was sharply decreased, indicating that •OH radicals was yet the dominated active species. Additionally, we also study the influence of H_2O_2 by the addition of Fe(II)-EDTA scavenger [54]. Noticeable, the PC efficiency (23.6%) of diclofenac was notably decreased, indicating that H_2O_2 was involved in the diclofenac degradation. Besides these, in order to evaluate the role of $\bullet O_2^-$ during PC process, *p*-benzoquinone (BQ) was used to scavenge the $\bullet O_2^-$ species [55]. As shown in Fig. 9, BQ exhibited considerably inhibition towards the PC degradation of diclofenac (19.9%). Moreover, with the addition of $K_2Cr_2O_7$ during the PC process [56], the PC efficiency of diclofenac (16.8%) was partial suppressed, suggesting that the role of electron (e^-) was lesser than that of H_2O_2 in our PC system. Thus, we can conclude that the PC degradation of diclofenac was mainly driven by the participation of •OH, e^- , $\bullet O_2^-$ and H_2O_2 , and to a lesser extent by the contribution of photoinduced h^+ radicals.

According to the aforementioned results, •OH radicals was yet the dominated species for degradation of diclofenac. Thus, in order to investigate the production rate of •OH radicals at photo-illuminated catalyst/water interface, highly fluorescent product of 2-hydroxyterephthalic acid (TAOH) which derived from the reaction between TPA and •OH radicals had been detected [57]. Fig. 10a exhibited the comparative fluorescence intensities of TAOH at 60 min on the pure TiO₂, r-TiO₂ and 4.25-Ag-Ag₂O/r-TiO₂-0.130 samples under visible light irradiation. Noticeable, Ag-Ag₂O/r-TiO₂ displayed the highest fluorescence intensity than that of others, revealing that 4.25-Ag-Ag₂O/r-TiO₂-0.130 nano-photocatalyst should possess the largest production amount of •OH radicals, which was ascribed to the more intense visible light absorbance

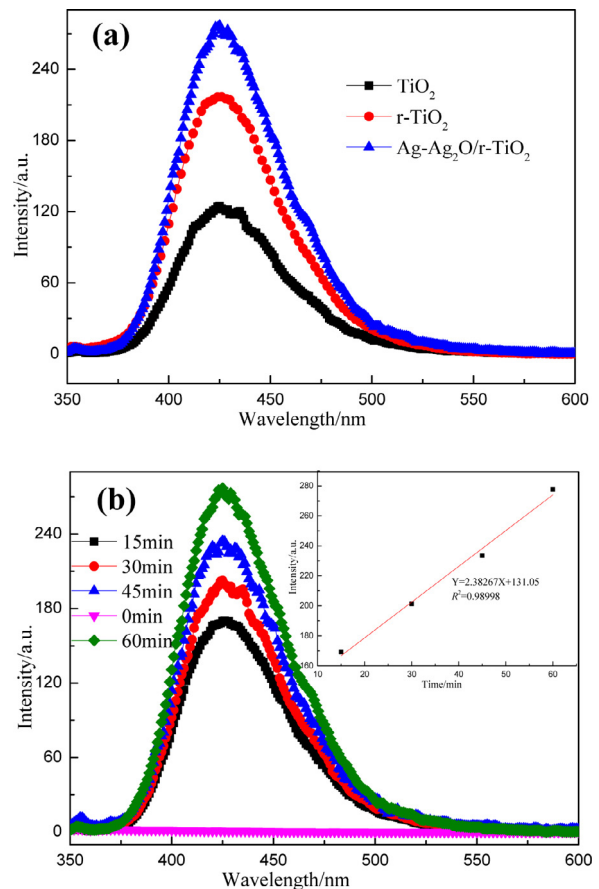


Fig. 10. Comparative fluorescence spectra (a) of pure TiO₂, r-TiO₂ and 4.25-Ag-Ag₂O/r-TiO₂-0.130 nano-photocatalysts under simulated sunlight irradiation and fluorescence spectra changes with visible light irradiation time (b) on 4.25-Ag-Ag₂O/r-TiO₂-0.130 nano-photocatalyst in a 0.5 mmol·L⁻¹ basic solution of terephthalic acid at 60 min. Inset of Fig. 10b showed the relationship between the corresponding fluorescence intensity of TAOH and irradiation time.

ability and higher separation efficiency of photoinduced charge carriers, meaning that 4.25-Ag-Ag₂O/r-TiO₂-0.130 sample should exhibit the highest VLD PC activity than those of others (Confirmed by Fig. 8a). Fig. 10b showed the evolution of fluorescence intensity of TAOH as a function of the duration of visible irradiation on 4.25-Ag-Ag₂O/r-TiO₂-0.130 nano-photocatalyst. Clearly, it can be detected that the fluorescence intensity at 425 nm increased gradually with prolonging the irradiation time. Besides, the fluorescence intensity of TAOH increased linearly with irradiation time (as displayed in the inset of Fig. 10b), suggesting that the •OH amount generated on the surface of 4.25-Ag-Ag₂O/r-TiO₂-0.130 was proportional to the irradiation time [58]. However, no TAOH signal was detected in the absence of the irradiation of 4.25-Ag-Ag₂O/r-TiO₂-0.130 sample.

3.6. Preliminary reaction mechanism

Based on the above systematic analysis, the enhanced VLD PC mechanism of Ag-Ag₂O/r-TiO₂ sample was proposed and illustrated in Fig. 11. In the present work, partly Ti⁴⁺ species in the lattice of TiO₂ was reduced by KBH₄ solution, thereby inducing the formation of Ti³⁺ self-doping energy level under the conduction band of TiO₂ semiconductor. Besides these, a trace of Ag⁺ species was also reduced to form Ag⁰ nanocrystalline with the help of KBH₄ solution. Thus, when the visible light irradiated the Ag-Ag₂O/r-TiO₂ nano-catalyst, electrons were easily migrated from the valence band to Ti³⁺ self-doping energy level. Furthermore, due to

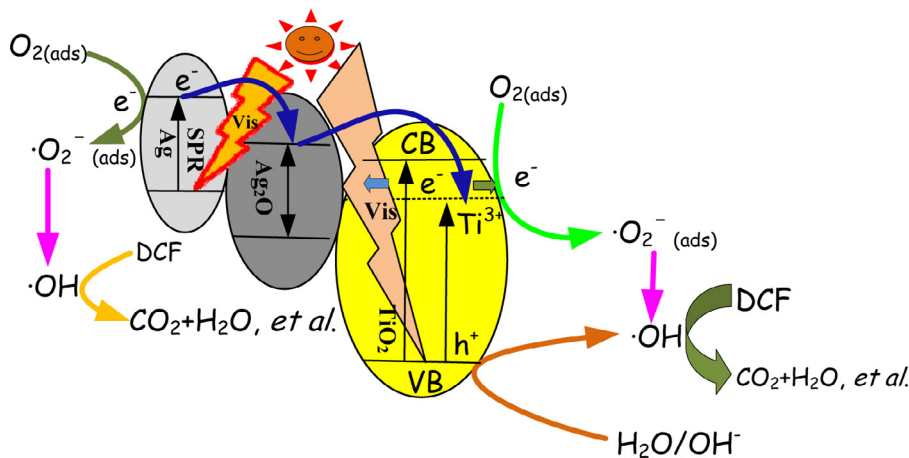


Fig. 11. Scheme of PC mechanism for Ag-Ag₂O/r-TiO₂ nano-photocatalyst.

the SPR effect of metallic Ag species, more visible light photons could be absorbed and then participate in the PC process, the photoinduced electrons could also migrate from valence band to the conduction band of Ag⁰ nanocrystalline. Subsequently, it is possible that the excited electrons can easily transfer from conduction band of Ag⁰ nanocrystalline to the surface of Ag₂O. Due to the positional relation of energy levels, the departed electrons transferred to the surface of Ti³⁺ self-doping energy level and conduction band of TiO₂. As a result, more photons could be utilized to participate in the PC reaction, resulting in a higher concentration of photoinduced charge carriers and PC efficiency. Finally, the departed photogenerated electrons and remaining holes could frequently react with the absorbed O₂ and H₂O molecules, respectively, forming the high active ·OH specie which responsible for the mineralization of contaminants (such as diclofenac in our case), leading to a high PC activity.

3.7. Stability

As we known, stability is very important to a photocatalyst during the industrial application for purification of refractory contaminants. Thus, in order to assess the stability and practicability of 4.25-Ag-Ag₂O/r-TiO₂-0.130, several consecutive PC experiments were performed. As displayed in Fig. 12, the PC performance kept at about a constant even after consecutive utilization for six recycles. Thus, we can conclude that Ag-Ag₂O/r-TiO₂ was stable, and it can be a potential candidate for the practical wastewater treatment and air purification.

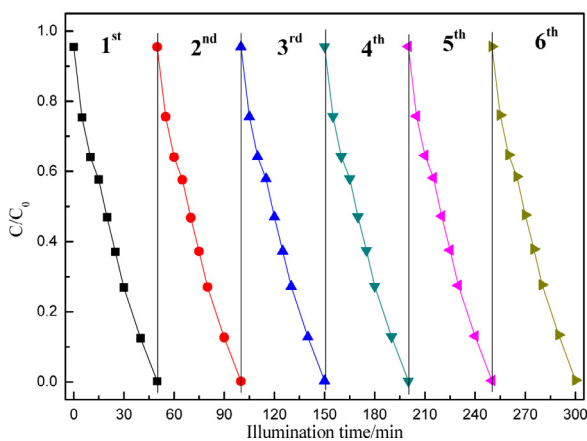


Fig. 12. The recycling numbers for PC degradation of diclofenac solution by 4.25-Ag-Ag₂O/r-TiO₂-0.130 nano-photocatalyst.

4. Conclusions

In summary, Ag-Ag₂O/r-TiO₂ nano-photocatalyst had been successfully fabricated through one-step solution reduction strategy in the presence of potassium borohydride, which could induce the simultaneously generation of Ti³⁺ self-doping energy level between the forbidden band of TiO₂ and metallic Ag species existed in the forms of Ag⁰ and Ag₂O nanocrystalline. In addition, the as-fabricated Ag-Ag₂O/r-TiO₂ displayed a significantly improved visible light absorbance ranging from 400 to 800 nm, higher photoinduced charge separation efficiency and larger production amount of ·OH radicals. Furthermore, Ag-Ag₂O/r-TiO₂ exhibited high VLD PC performance for degradation of diclofenac, which was mainly attributed to the localized SPR of Ag⁰ nanocrystalline, intense visible light absorbance and efficient charge separation. This study would provide a facile and feasible strategy to fabricate VLD nano-catalyst which could be applied in the fields of waste water treatment, air purification, sensors and solar energy utilization.

Acknowledgements

This work was kindly supported by National Natural Science Foundation of China (51508254), Nature Science Foundation of Gansu Province of China (1506RJZA216), Fundamental Research Funds for the Central Universities (lzujbky-2015-137) and Opening Project of State Key Laboratory of High Performance Ceramics and Superfine Microstructure (SKL201509SIC).

Appendix A. Supplementary data

Supplementary data associated with this article can be found, in the online version, at <http://dx.doi.org/10.1016/j.apcatb.2017.01.014>.

References

- [1] A. Fujishima, K. Honda, Electrochemical photolysis of water at a semiconductor electrode, *Nature* 238 (1972) 37–38.
- [2] P. Pichat, J. Disdier, C. Hoang-Van, D. Mas, G. Goutailler, C. Gayssé, Purification/deodorization of indoor air and gaseous effluents by TiO₂ photocatalyst, *Catal. Today* 63 (2000) 363–369.
- [3] M. Grätzel, Photoelectrochemical cells, *Nature* 414 (2001) 338–344.
- [4] E.Y. Bae, W.Y. Choi, Highly enhanced photoreductive degradation of perchlorinated compounds on dye-sensitized metal/TiO₂ under visible light, *Environ. Sci. Technol.* 37 (2003) 147–152.
- [5] M. Linsebigler, G.Q. Lu, Y.T. Yates, Photocatalysis on TiO₂ surfaces: principles, mechanisms, and selected results, *Chem. Rev.* 95 (1995) 735–758.

- [6] S.K. Joung, T. Amemiya, M. Murabayashi, K. Itoh, Mechanistic studies of the photocatalytic oxidation of trichloroethylene with visible-light-driven N-doped TiO₂ photocatalysts, *Chem. Eur. J.* 12 (2006) 5526–5534.
- [7] R.P. Vitiello, J.M. Macak, A. Ghicov, H. Tsuchiyua, L.F.P. Dick, P. Schmuki, N-doping of anodic TiO₂ nanotubes using heat treatment in ammonia, *Electrochim. Commun.* 8 (2006) 544–548.
- [8] X.W. Cheng, G.P. Pan, X.J. Yu, T. Zheng, Preparation of CdS NCs decorated TiO₂ nano-tubes arrays photoelectrode and its enhanced photoelectrocatalytic performance and mechanism, *Electrochim. Acta* 105 (2013) 535–541.
- [9] W. Choi, A. Termin, M.R. Hoffman, The role of metal ion dopant in quantum-sized TiO₂: correlation between photoreactivity and charge carrier recombination dynamics, *J. Phys. Chem.* 98 (1994) 13669–13679.
- [10] D. Buso, J. Pacifico, A. Martucci, P. Mulvaney, Gold-nanoparticle-doped TiO₂ semiconductor thin films: optical characterization, *Adv. Funct. Mater.* 17 (2007) 347–354.
- [11] J.G. Wang, P. Zhang, X. Li, J. Zhu, H.X. Li, Synchronical pollutant degradation and H₂ production on a Ti³⁺-doped TiO₂ visible photocatalyst with dominant {001} facets, *Appl. Catal. B: Environ.* 134–135 (2013) 198–204.
- [12] W.Z. Fang, M.Y. Xing, J.L. Zhang, A new approach to prepare Ti³⁺ self-doped TiO₂ via NaBH₄ reduction and hydrochloric acid treatment, *Appl. Catal. B: Environ.* 160–161 (2014) 240–246.
- [13] T.L. Thompson, J.T. Yates Jr., Surface science studies of the photoactivation of TiO₂-new photochemical processes, *Chem. Rev.* 106 (2006) 4428–4453.
- [14] N.S. Portillo-Vélez, O. Olvera-Neria, I. Hernández-Pérez, A. Rubio-Ponce, Localized electronic states induced by oxygen vacancies on anatase TiO₂ (101) surface, *Surf. Sci.* 616 (2013) 115–119.
- [15] H. Zhou, Y.R. Zhang, Enhancing the capacitance of TiO₂ nanotube arrays by a facile cathodic reduction process, *J. Power Sources* 23 (2013) 128–131.
- [16] Q. Kang, J.Y. Cao, Y.J. Zhang, L.Q. Liu, H. Xu, J.H. Ye, Reduced TiO₂ nanotube arrays for photoelectrochemical water splitting, *J. Mater. Chem. A* 1 (2013) 5766–5774.
- [17] X.W. Cheng, Q.F. Cheng, B. Li, X.Y. Deng, J.J. Li, P. Wang, B.Q. Zhang, H.L. Liu, X.N. Wang, One-step construction of N/Ti³⁺ codoped TiO₂ nanotubes photoelectrode with high photoelectrochemical and photoelectrocatalytic performance, *Electrochim. Acta* 186 (2015) 442–448.
- [18] X.X. Hu, C. Hu, T.W. Peng, X.F. Zhou, J.H. Qu, Plasmon-induced inactivation of enteric pathogenic microorganisms with Ag-AgI/Al₂O₃ under visible-light irradiation, *Environ. Sci. Technol.* 44 (2010) 7058–7062.
- [19] D. Tsukamoto, Y. Shiraiishi, Y. Sugano, S. Ichikawa, S. Tanaka, T. Hirai, Gold nanoparticles located at the interface of anatase/rutile TiO₂ particles as active plasmonic photocatalysts for aerobic oxidation, *J. Am. Chem. Soc.* 134 (2012) 6309–6315.
- [20] R.H. Li, W.X. Chen, H. Kobayashi, C.X. Ma, Platinum-nanoparticle-loaded bismuth oxide: an efficient plasmonic photocatalyst active under visible light, *Green Chem.* 10 (2010) 212–215.
- [21] Y. Hou, F. Zuo, Q. Ma, C. Wang, L. Bartels, P.Y. Feng, Ag₃PO₄ oxygen evolution photocatalyst employing synergistic action of Ag/AgBr nanoparticles and graphene sheets, *J. Phys. Chem. C* 116 (2012) 20132–20139.
- [22] L.S. Zhang, K.H. Wong, H.Y. Yip, C. Hu, J.C. Yu, C.Y. Chan, P.K. Wong, Effective photocatalytic disinfection of *E. coli* K-12 using AgBr-Ag-Bi₂WO₆ nanojunction system irradiated by visible light: the role of diffusing hydroxyl radicals, *Environ. Sci. Technol.* 44 (2010) 1392–1398.
- [23] M.S. Zhu, P.L. Chen, M.H. Liu, Graphene oxide enwrapped Ag/AgX (X = Br, Cl) nanocomposite as a highly efficient visible-light plasmonic photocatalyst, *ACS Nano* 5 (2011) 4529–4536.
- [24] Y. Hou, X.Y. Li, Q.D. Zhao, G.H. Chen, C.L. Raston, Role of hydroxyl radicals and mechanism of *Escherichia coli* inactivation on Ag/AgBr/TiO₂ nanotube array electrode under visible light irradiation, *Environ. Sci. Technol.* 46 (2012) 4042–4050.
- [25] C.L. Wu, Facile one-step hydrothermal synthesis of Ag/Ag₂O/Ag₂CO₃ microcomposite with visible light-driven photocatalytic activity, *Mater. Lett.* 160 (2015) 291–293.
- [26] Z.J. Yan, R.Q. Ren, D.B. Chrisey, Generation of Ag-Ag₂O complex nanostructures by excimer laser ablation of Ag in water, *Phys. Chem. Chem. Phys.* 15 (2013) 3052–3056.
- [27] M.X. Sun, X.L. Cui, Anodically grown Si-W codoped TiO₂ nanotubes and its enhanced visible light photoelectrochemical response, *Electrochim. Commun.* 20 (2012) 133–136.
- [28] P. Hájková, J. Matoušek, P. Antoš, Aging of the photocatalytic TiO₂ thin films modified by Ag and Pt, *Appl. Catal. B: Environ.* 160–161 (2014) 51–56.
- [29] R. Asahi, T. Morikawa, T. Ohwaki, K. Aoki, Y. Taga, Visible-light photocatalysis in nitrogen-doped titanium oxides, *Science* 293 (2001) 269–271.
- [30] Y.B. Luan, L.Q. Jing, J. Wu, M.Z. Xie, Y.J. Feng, Long-lived photogenerated charge carriers of 001-facet-exposed TiO₂ with enhanced thermal stability as an efficient photocatalyst, *Appl. Catal. B: Environ.* 147 (2014) 29–34.
- [31] M.Z. Xie, X.D. Fu, L.Q. Jing, P. Luan, Y.J. Feng, H.G. Fu, Long-lived visible-light-excited charge carriers of TiO₂/BiVO₄ nanocomposites and their unexpected photoactivity for water splitting, *Adv. Energy Mater.* 4 (2014) 1300995.
- [32] Y.L. Zhang, S. Wei, H.Y. Zhang, S. Liu, F. Nawaz, F.S. Xiao, Nanoporous polymer monoliths as adsorptive supports for robust photocatalyst of Degussa P25, *J. Hazard. Mater.* 339 (2009) 434–438.
- [33] J.G. Yu, G.P. Dai, B. Cheng, Effect of crystallization methods on morphology and photocatalytic activity of anodized TiO₂ nanotube array films, *J. Phys. Chem. C* 114 (2010) 19378–19385.
- [34] M. Thenmozhi, K. Kannabiran, R. Kumar, V. Gopesh Khanna, Antifungal activity of Streptomyces sp. VITSTK7 and its synthesized Ag₂O/Ag nanoparticles against medically important Aspergillus pathogens, *J. Mycol. Méd.* 23 (2013) 97–103.
- [35] J.B. Chen, H.N. Che, K. Huang, C.B. Liu, W.D. Shi, Fabrication of a ternary plasmonic photocatalyst CQDs/Ag/Ag₂O to harness charge flow for photocatalytic elimination of pollutants, *Appl. Catal. B: Environ.* 192 (2016) 134–144.
- [36] D.S. Guan, J.Y. Li, X.F. Gao, C. Yuan, Controllable synthesis of MoO₃-deposited TiO₂ nanotubes with enhanced lithium-ion intercalation performance, *J. Power Sources* 246 (2014) 305–312.
- [37] Y.J. Xin, H.L. Liu, J.J. Li, Q.H. Chen, D. Ma, Influence of post-treatment temperature of TNTa photoelectrodes on photoelectrochemical properties and photocatalytic degradation of 4-nonylphenol, *J. Solid State Chem.* 199 (2013) 49–55.
- [38] L. Wang, A. Teleki, S.E. Pratsinis, P.I. Gouma, Ferroelectric WO₃ nanoparticles for acetone selective detection, *Chem. Mater.* 20 (2008) 4794–4796.
- [39] X.W. Cheng, Q.F. Cheng, X.Y. Deng, P. Wang, H.L. Liu, Construction of TiO₂ nano-tubes arrays coupled with Ag₂S nano-crystallites photoelectrode and its enhanced visible light photocatalytic performance and mechanism, *Electrochim. Acta* 184 (2015) 264–275.
- [40] S.S. Liu, N. Wang, Y.C. Zhang, Y.R. Li, Z. Han, P. Na, Efficient removal of radioactive iodide ions from water by three-dimensional Ag₂O-Ag/TiO₂ composites under visible light irradiation, *J. Hazard. Mater.* 284 (2015) 171–181.
- [41] A.I. Boronin, S.V. Koscheev, G.M. Zhidomirov, XPS and UPS study of oxygen states on silver, *J. Electron Spectrosc. Relat. Phenom.* 96 (1998) 43–51.
- [42] X.W. Cheng, Q.F. Cheng, X.Y. Deng, P. Wang, H.L. Liu, A facile and novel strategy to synthesize reduced TiO₂ nanotubes photoelectrode for photoelectrocatalytic degradation of diclofenac, *Chemosphere* 144 (2016) 888–894.
- [43] M.A. Henderson, W.S. Epling, C.H.F. Peden, C.L. Perkins, Insights into photoexcited electron scavenging processes on TiO₂ obtained from studies of the reaction of O₂ with oh groups adsorbed at electronic defects on TiO₂ (110), *J. Phys. Chem. B* 107 (2003) 534–545.
- [44] X.W. Cheng, H.L. Liu, Q.H. Chen, J.J. Li, P. Wang, Preparation of graphene film decorated TiO₂ nano-tube array photoelectrode and its enhanced visible light photocatalytic mechanism, *Carbon* 66 (2014) 450–458.
- [45] X.W. Cheng, X.J. Yu, Z.P. Xing, One-step synthesis of Fe-N-S-tri-doped TiO₂ catalyst and its enhanced visible light photocatalytic activity, *Mater. Res. Bull.* 47 (2012) 3804–3809.
- [46] F. Zuo, L. Wang, T. Wu, Z.Y. Zhang, D. Borchardt, P.Y. Feng, Self-doped Ti³⁺ enhanced photocatalyst for hydrogen production under visible light, *J. Am. Chem. Soc.* 132 (2010) 11856–11857.
- [47] W.Z. Fang, M.Y. Xing, J.L. Zhang, A new approach to prepare Ti³⁺ self-doped TiO₂ via NaBH₄ reduction and hydrochloric acid treatment, *Appl. Catal. B: Environ.* 160–161 (2014) 240–246.
- [48] Y.H. Lin, D.J. Wang, Q.D. Zhao, M. Yang, Q.L. Zhang, A study of quantum confinement properties of photogenerated charges in ZnO nanoparticles by surface photovoltaic spectroscopy, *J. Phys. Chem. B* 108 (2004) 3202–3206.
- [49] L.Q. Jing, X.J. Sun, J. Shang, W.M. Cai, Z.L. Xu, Y.G. Du, H.G. Fu, Review of surface photovoltaic spectra of nano-sized semiconductor and its applications in heterogeneous photocatalysis, *Sol. Energy Mater. Sol. Cells* 79 (2003) 133–151.
- [50] X. Wei, T.F. Xie, L.L. Peng, W. Fu, J.S. Chen, Q. Gao, G.Y. Hong, D.J. Wang, Effect of heterojunction on the behavior of photogenerated charges in Fe₃O₄@Fe₂O₃ nanoparticle photocatalysts, *J. Phys. Chem. C* 115 (2011) 8637–8642.
- [51] M.R. Hoffman, S.T. Martin, W.Y. Chio, D.W. Bahnemann, Environmental application of semiconductor photocatalysis, *Chem. Rev.* 95 (1995) 69–96.
- [52] W.J. Li, D.Z. Li, W.J. Zhang, Y. Hu, Y.H. He, X.Z. Fu, Microwave synthesis of Zn_xCd_{1-x}S nanorods and their photocatalytic activity under visible light, *J. Phys. Chem. C* 114 (2010) 2154–2159.
- [53] Y.M. Lin, D.Z. Li, J.H. Hu, G.C. Xiao, J.X. Wang, W.J. Li, X.Z. Fu, Highly efficient photocatalytic degradation of organic pollutants by PANI-modified TiO₂ composite, *J. Phys. Chem. C* 116 (2012) 5764–5772.
- [54] Y.M. Chen, A.H. Lu, Y. Li, L.S. Zhang, H.Y. Yip, H.J. Zhao, T.C. An, P.K. Wong, Naturally occurring sphalerite as a novel cost-effective photocatalyst for bacterial disinfection under visible light, *Environ. Sci. Technol.* 45 (2011) 5689–5695.
- [55] L.Q. Ye, J.Y. Liu, C.Q. Gong, L.H. Tian, T.Y. Peng, L. Zan, Two different roles of metallic Ag on Ag/AgX/BiOX (X = Cl, Br) visible light photocatalysts: surface plasmon resonance and Z-scheme bridge, *ACS Catal.* 2 (2012) 1677–1683.
- [56] T.C. An, J.B. An, H. Yang, G.Y. Li, H.X. Feng, X.P. Nie, Photocatalytic degradation kinetics and mechanism of antivirus drug-lamivudine in TiO₂ dispersion, *J. Hazard. Mater.* 197 (2011) 229–236.
- [57] K. Ishibashi, A. Fujishima, T. Watanabe, K. Hashimoto, Detection of active oxidative species in TiO₂ photocatalysis using the fluorescence technique, *Electrochim. Commun.* 2 (2000) 207–210.
- [58] Y.Y. Song, P. Roy, I. Paramasivan, P. Schmuki, Voltage-induced payload release and wettability control on TiO₂ and TiO₂ nanotubes, *Angew. Chem. Int. Ed.* 49 (2010) 351–354.